Electrical Characterization of Al/Ta_2O_5/Al Structures Grown by Electron Beam Deposition

I.S. Yahia[a,b,*] and A.A.M. Farag[c]

[a]Department of Physics, Center of Excellent for Advanced Materials Research, Faculty of Science, King Khalid University, P.O. Box 9004, Abha, Saudi Arabia

[b]Nano-Science&Semiconductor Labs., Physics Department, Faculty of Education, Ain Shams University Roxy, Cairo, Egypt

[c]Thin Film Laboratory, Department of Physics, Faculty of Education, Ain Shams University, Roxy, Cairo, Egypt

(Received April 28, 2013; in final form February 20, 2014)

We report study of current density–voltage (J–V) and capacitance–voltage (C–V) characteristics of Al/Ta_2O_5/Al metal–insulator–metal structures prepared by electron beam deposition. At low bias voltages the J–V characteristics of Al/Ta_2O_5/Al structures show ohmic conduction. At higher voltages the conductivity becomes limited by space charge. The space charge limited conductivity is due to carrier trap centers located within the energy gap of Ta_2O_5. The distribution of the trap appears to be exponential above the valence band. Basing on the comparison of the measured temperature dependences of the current density with the theoretical model one can determine important material parameters, such as the trap density. The density of states at the Fermi level $N(E_F)$ for the Ta_2O_5 film is found to be 2.75×10^{19} eV^{-1} cm^{-3}. The capacitance–voltage–temperature (C–V–T) characteristics of Al/Ta_2O_5/Al structures were carried out in the bias range -5 to $+5$ V and at temperatures from 300 to 550 K. The capacitance of Al/Ta_2O_5/Al structures increases with the increasing temperature.

DOI: 10.12693/APhysPolA.125.1191

PACS: 77.84.Bw, 77.55.–g, 81.10.Bk, 85.30.Kk, 85.30.–z

1. Introduction

With a rapid development of semiconductor industry increases a demand for materials which can be integrated into memory devices and advanced electronic packaging applications as capacitors. Because of that investigations of such material parameters as values of dielectric constant, leakage current densities, breakdown field strengths, and effect of frequency or temperature on dielectric constants focus recently significant attention [1, 2].

Ditantalum pentoxide (Ta_2O_5) is known for its relatively high dielectric constant (about 25), good chemical and thermal stability and compatibility with standard microelectronic processing operations. This material has been used as a discrete capacitor insulator in electronic applications, as an oxygen sensor, and as a high-temperature resistor [3, 4]. The recent study of its ionic conductivity has also demonstrated its performance as an ionic membrane or a solid electrolyte in multilayered electrochromic devices [5]. Thus, thin ditantalum pentoxide films become potentially important in microelectronics. They are regarded as promising candidates for capacitor insulators in high density dynamic random access memories (DRAMs) [6–8]. Moreover, the Ta_2O_5 films are of interest for applications in optical waveguides, antireflection coatings, and MOS devices. Up to now, the study of the optical properties of Ta_2O_5 has been focused on material absorption or waveguide attenuation [9–12]. From the point of view of optical applications Ta_2O_5 thin films exhibit many attractive properties, including the high optical transmission, high refractive index, good thermal and chemical stability, and good barrier properties. The properties have a wide variety of applications, e.g., as an anti-reflection coating for solar cells [13], wave guides for surface acoustic devices [14], interference and protective coatings for optical filters and lenses [15], and dielectrics in electrochromic devices requiring high permittivity [16, 17].

In this study, ditantalum pentoxide (Ta_2O_5) thin films deposited on BK7 glass substrates by electron beam deposition have been characterized by electrical methods. The electrical properties of Al/Ta_2O_5/Al metal–insulator–metal (MIM) structures were studied in current density–voltage and capacitance–voltage measurements in a wide range of temperatures. The parameters extracted from J–V and C–V characteristics were interpreted basing on theoretical models developed for transport properties in this kind of structures.

2. Experimental

Ditantalum pentoxide Ta_2O_5 films were deposited by electron beam deposition technique in a high vacuum chamber on BK7 glass substrates. The deposition process was carried out at room temperature. For the deposition the A700QE-Leybold Optics electron beam deposition system with the base pressure of 8×10^{-6} mbar was employed. The BK7 glass surfaces were treated by very fine polishing and cleaning to assure high quality of the Ta_2O_5 thin films. For the film evaporation we

*corresponding author; e-mail: dr_isyahia@yahoo.com, ihussein@kku.edu.sa, isyahia@gmail.com

used Ta_2O_5 powder of 99.99% purity supplied by Umicore Materials AG. The evaporation rate was adjusted to 0.5 nm/s. The rate and the final layer thickness were controlled by quartz crystal deposition monitor (model type IC/5). During the evaporation of the materials, the reactive process with oxygen O_2 was carried out at pressure 2.5×10^{-4} mbar. The thickness of the deposited Ta_2O_5 was $d = 0.67$ μm.

The structural characterization of Ta_2O_5 thin film was carried out by using X-ray diffraction. Philips X-ray diffractometer (model X'-Pert) was used for the measurements. The absence of sharp peaks in the X-ray patterns indicates that the Ta_2O_5 films are amorphous in agreement with previous observations by Azim et al. [18].

The current density–voltage (J–V) characteristics on Al/Ta_2O_5/Al MIM devices were measured using a high internal impedance electrometer type Keithley 617A Source/Measure unit for dc measurement via equipped suitable coaxial cable. Capacitance–voltage measurements were performed using a computer controlled 410 C–V meter with an operating frequency of 1 MHz interfaced via model 4108 C–V interface. This system includes a 1 MHz capacitance meter, variable dc voltage for bias stressing, ramp generator-programmer. Front-panel programming controls allow the voltage applied to the device to ramp between adjustable Start and Stop limits at the desired rate. The 410, in conjunction with an X–Y recorder, produces real-time C–V plots. These measurements were performed under a forward and reverse biasing voltage. The temperature of the device was controlled using chromel–alumel thermocouple (Type-K) connected to temperature controller (type termotronic), Scotti instruments, Italy.

3. Results and discussions

3.1. J–V characteristics of Al/Ta_2O_5/Al structure

The dependences of current density (J) on voltage (V) measured at various temperatures in the range 300–550 K is shown in Fig. 1 using the double logarithmic scale for a typical A/Ta_2O_5/Al structure. Each J–V curve exhibits two distinct voltage regions. In the lower voltage region, the slopes of the curves are approximately equal to unity, i.e., J is directly proportional to V ($J \approx V^m$, $m \approx 1$). This behavior is simply described by Ohm's law. This gives evidence that the injected carrier density is lower than the thermally generated carrier density. When the injected carrier density is greater than the free carrier density, the current becomes space charge limited.

For higher bias voltages, the current density is described by the power law $J \approx V^m$ ($2.5 < m < 3.5$) indicating the onset of space charge limited conduction (SCLC) [19]. This result contradicts the $J \approx V^2$ behavior reported by McKenzie and coworkers [20] which was explained by a single trap model [21]. A fairly well-defined transition voltage (V_t) can be derived from each characteristic by obtaining the intersection point of the two linear sections of the logarithmic characteristics at x-axis. As shown in Fig. 2, the transition voltage V_t decreases with the increasing temperature. This behavior

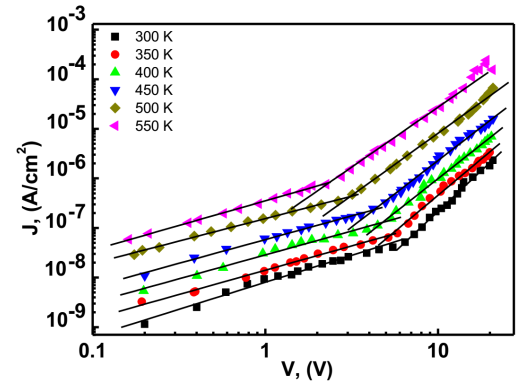

Fig. 1. J–V characteristics (log – log scale) for Al/Ta_2O_5/Al MIM device at different temperatures.

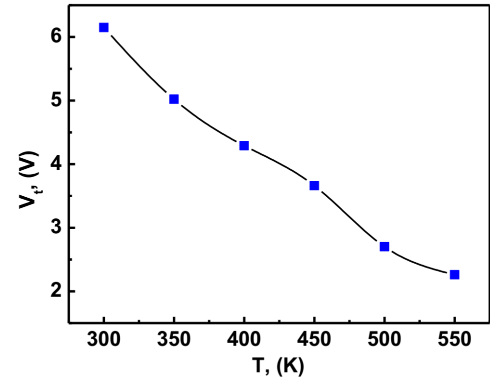

Fig. 2. Temperature dependence of the transition voltage V_t for Al/Ta_2O_5/Al MIM structure.

may be attributed to the decrease of the density of the structural defects [22].

The existence of the second region of J–V characteristics suggests a SCLC mechanism, with exponential trap distribution. The slope m in the second region decreases with increasing temperature. The temperature dependence of the exponent m is shown in Fig. 3. The observed

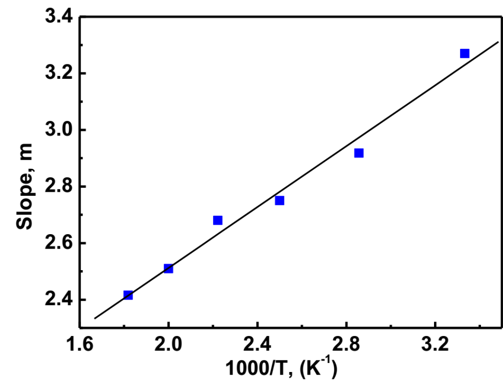

Fig. 3. Plot of the slope m versus $1000/T$ for Al/Ta_2O_5/Al MIM structure.

proportionality confirms a SCLC model controlled by an exponential distribution of traps [5]. This type of conduction can be expressed as [23, 24]:

$$J = \frac{e\mu N_v}{d^{2l+1}}\left(\frac{\varepsilon\varepsilon_0}{eP_0kT_t}\right)^l V^{l+1}, \tag{1}$$

where ε is the dielectric constant of the semiconductor, ε_0 is the permitivity of free space, e is the electronic charge, μ is the mobility of carrier charges, N_v is the effective density of states in valence band edge, d is the thickness of the sample, l is a parameter given by $l = T_t/T$, T_t is a characteristic temperature of the exponential distribution of the traps. The total density of trap states is given by [23, 24]:

$$N_t = P_0kT_t, \tag{2}$$

where P_0 is the trap density per unit energy range at the valence band. The exponential trapping distribution is given by [23, 24]:

$$P(E) = P_0 \exp\left(\frac{-E}{kT_t}\right), \tag{3}$$

where E is the energy above the valence band edge. The slopes of curves (m) as shown in Fig. 3 were determined to be equal to $l+1$. T_t value was calculated from these curves as 538 K. It is seen that T_t values change with temperature.

Temperature–current density–voltage measurements allow the determination of additional information concerning the film material. On the basis of Eqs. (1) and (2), Gould [25] has shown that plots of $\log(J)$ vs. $1000/T$ at constant voltages in the SCLC region are straight lines. The gradient of the plots is given by [25]:

$$\frac{\mathrm{d}(\log J)}{\mathrm{d}(1/T)} = T_t \log\left(\frac{\varepsilon\varepsilon_0}{ed^2N_t}\right). \tag{4}$$

The slope varies with voltage and yields a value for N_t. Figure 4 shows typical examples of such curves for the Al/Ta$_2$O$_5$/Al structure at constant applied voltages equal to 8, 12, 16, and 20 V. On extrapolation, it is predicted that all $\log(J)$ vs. $1000/T$ plots should intercept at a common point, whose coordinates are given by [25]:

$$\log(J) = \log\left(\frac{e^2\mu dN_vN_t}{\varepsilon\varepsilon_0}\right), \quad \frac{1}{T} = \frac{1}{T_t}. \tag{5}$$

These coordinates are independent of the bias voltages applied to the films. The values of N_t could be (again) obtained using the coordinates of the intersection point in Fig. 4. The values of N_t obtained in the range of 2.28×10^{20} m^{-3}. The trap density per unit energy range at the valence band P_0 and the charge mobility μ can easily be determined and were found to be 3.05×10^{40} J^{-1} m^{-3} and 2.85 m^2/(V s), respectively.

By determining both T_t and P_0 and combining them with Eq. (3), the trap density per unit energy range at an energy E above the valence band edge could be evaluated, using Eq. (3), and the obtained data are shown in Fig. 5. This figure exhibits a decrease in $P(E)$ with increase of the value of the energy above the valence band edge and this may be due to the decrease in the scattering centers as the film thickness increases [22].

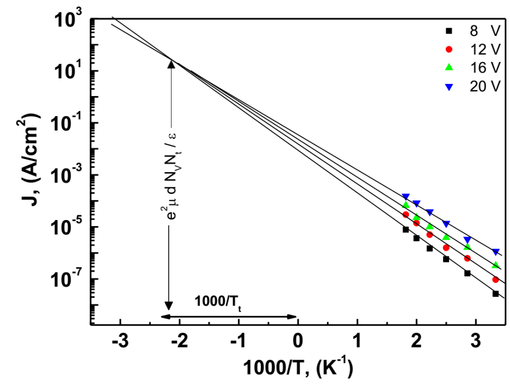

Fig. 4. Plot of the current density J versus $1000/T$ for Al/Ta$_2$O$_5$/Al MIM device at different applied voltages.

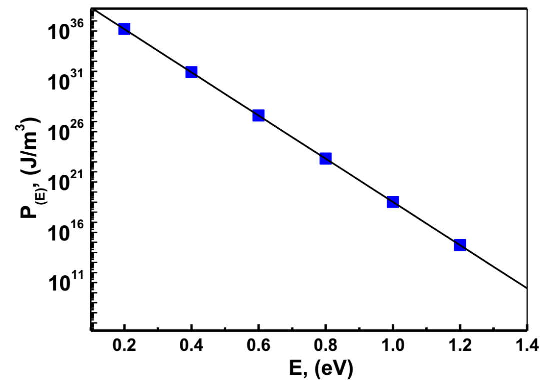

Fig. 5. The variation of $\log P(E)$ with energy E for Al/Ta$_2$O$_5$/Al MIM device.

According to the theory of the space charge-limited conduction, in the case of uniform distribution of localized states, the current density at a particular voltage (V) is given by the following relation [26, 27]:

$$J = KV \exp(SV), \tag{6}$$

where K is a constant and can be expressed as [26, 27]:

$$K = \frac{e\mu n}{d}, \tag{7}$$

where n is the carrier concentration (density of thermally activated charge carriers). The value of n was determined from the intercept of $\log(J/V)$ vs. V for each temperature and plotted as a function of temperature and shown in Fig. 6. As the temperature is increased, the number of broken bonds (carriers) in the material increases because there is more thermal energy available so more and more electrons gain enough energy to break free [28].

In Eq. (6), S is the slope of $\log(J/V)$ vs. V plot and can be given by the following form [26]:

$$S = \frac{2\varepsilon\varepsilon_0}{eN(E_f)kTd^2}, \tag{8}$$

where $N(E_f)$ is the density of localized states near the

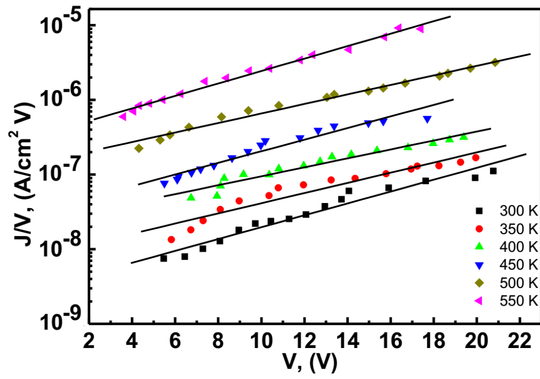

Fig. 6. Semilogarithmic plots of J/V versus V for Al/Ta_2O_5/Al MIM device at different temperatures.

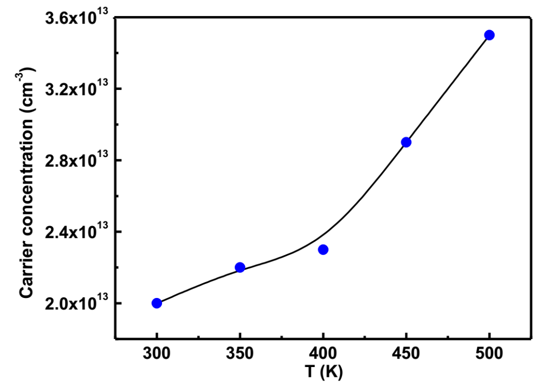

Fig. 8. Plot of carrier concentration versus T for Al/Ta_2O_5/Al MIM structure.

Fermi level, ε is the dielectric constant of the sample, ε_0 is the permittivity of free space and k is the Boltzmann constant. As evident from Eqs. (6) and (7), in the case of space charge limited conduction, the $\log J/V$ versus V curves should be a straight line and the slope (S) of these curves should be inversely proportional to the temperature. The plots of $\log(J/V)$ versus V at different temperatures in the range 300–550 K were plotted as shown in Fig. 6. Values of S were obtained from the slope of these curves. $N(E_F)$ value was determined from the slope of S vs. $1000/T$ plot (Fig. 7) and was found as 2.75×10^{19} eV^{-1} cm^{-3}. It is seen that S values are proportional to the inverse of temperature. S values were found to decrease with increasing temperature. The obtained results show the presence of space charge limited conduction. As the temperature increases, the trapped carriers are thermally activated to the conduction band. The linear fitting in Fig. 7 suggests that the high-electric conduction region is governed by the space charge. Furthermore, interfacial layer between Al metal and Ta_2O_5 causes a voltage drop across the interface and thus, the voltage dependence of the reverse current can be explained by the drop over an interfacial oxide layer [29].

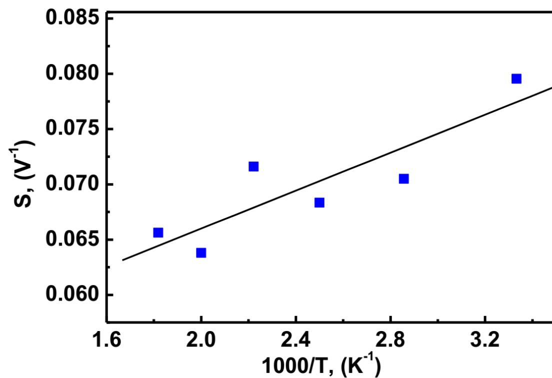

Fig. 7. Plot of the slope S versus $1000/T$ for Al/Ta_2O_5/Al MIM structure.

The carrier concentration in Ta_2O_5 was calculated using the determined carrier mobility at different temperatures and plotted as a function of temperature as shown in Fig. 8.

3.2. Capacitance–voltage characteristics at different temperatures for Al/Ta_2O_5/Al MIM structure

The measured high frequency C–V characteristics as a function of biasing voltage for Al/Ta_2O_5/Al MIM structure in the temperature range of 300–550 K are shown in Fig. 9. The frequency and the amplitude of the ac signal were 1 MHz and 40 mV$_{\rm rms}$ and the dc bias voltage swept from -5 to 5 V. It is observed that the C–V characteristics are dependent on bias polarity. When the negative bias is applied ($-2 > V > 0$) on the top of Al-electrode, noticeable voltage dependent of the capacitance is obtained for all the measured temperature than those with a positive bias applied. This capacitance–voltage dependence is believed to relate with the existence of bulk-dielectric traps near the dielectric/metallic interface [30]. At which, different traps will induce charges with different time constants and modulate capacitor charges.

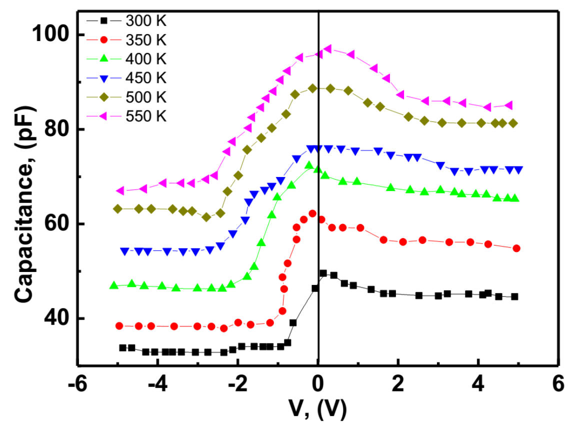

Fig. 9. Plot of the C–V characteristics for Al/Ta_2O_5/Al MIM device at different temperature.

In addition, Green and Shewchun [31] show that the strong minority injection from the metal contact causes large value of C in the C–V characteristic, and for the large barrier with a reasonably thick insulator the minority-carrier current dominates the majority-carrier current. They also showed that the minority-carrier device has a top metal contact having a metal-to-insulator barrier height, which has been found experimentally to roughly correspond to aluminum [32].

It is well known that for a parallel plate capacitor, the capacitance is proportional to the electrode area and the reversed dielectric thickness. Similarly, the capacitance of a coplanar capacitor is also dependent on the electrode area ($W \times L$) and electrode gap (t). In our work, the device is often made with $L \gg W$ and W being kept as a constant value; i.e. the electrode area is proportional to L. In that case, one can reasonably assume that the capacitance is proportional to L. Our experiment has confirmed that the capacitance and the area of electrode follows a nonlinear relationship; i.e. $C \propto (A)^n$, where n is smaller than unity and approximately ≈ 0.65. Moreover, the capacitance decreases as the gap becomes wider; empirically the data can be fitted as $C \propto (1/t)^m$ where $m \approx 0.3$ [33–36]. In the case of application of an alternating voltage across a certain semiconducting material, the equivalent capacitance measured by a C–V meter is given by [33–37]:

$$C = \left(\frac{A^n \sigma_{\mathrm{AC}}}{t^m}\right)\left(\tau_{\mathrm{m}} - \frac{\tau}{1+\omega^2\tau^2}\right), \quad (9)$$

where $\tau_{\mathrm{m}} = \frac{\varepsilon\varepsilon_0}{\sigma_{\mathrm{AC}}}$ is the Maxwellian dielectric relaxation time, ε is the dielectric constant of Ta_2O_5 film, ε_0 is the permittivity of free space, and τ is the dielectric relaxation time. After substituting τ_{m}, Eq. (9) can be written as

$$C = \left(\frac{\varepsilon\varepsilon_0 A^n}{t^m}\right)\left(1 - \frac{\tau\sigma_{\mathrm{AC}}}{\varepsilon\varepsilon_0(1+\omega^2\tau^2)}\right). \quad (10)$$

Due to the lower conductivity of Ta_2O_5 film, then the second term of Eq. (10) can be ignored and the capacitance is given by

$$C = \frac{\varepsilon\varepsilon_0 A^n}{t^m}. \quad (11)$$

Figure 10 shows the capacitance variation of Al/Ta_2O_5/Al MIM structure as function of temperature for different applied biasing voltages at 1 MHz. The results for all biases show that the capacitance increases with increase of temperature in agreement with those published before by Hu et al. [30]. This behavior may be attributed to the increase in carrier concentration as the temperature increases.

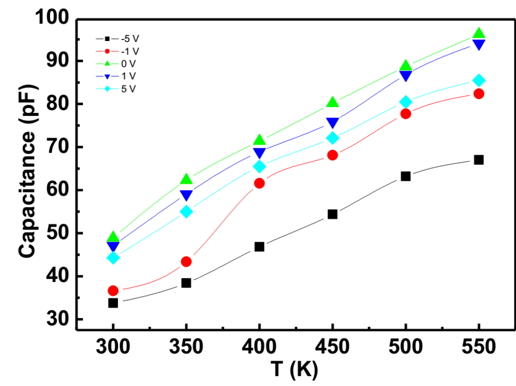

Fig. 10. Plot of the C–T characteristics for Al/Ta_2O_5/Al MIM device at different applied biasing voltage.

4. Conclusions

The SCLC mechanism in Al/Ta_2O_5/Al structure was investigated at different temperatures in the range 300–550 K. The J–V curves of the diode exhibit two regions, which correspond to ohmic conduction and space charge limited conduction mechanisms. A fairly well-defined transition voltage V_{t} can be derived from each characteristic. The slope m of second region decreases linearly with increasing temperature. This linearity confirms a SCLC model controlled by an exponential distribution of traps. The density of localized states for the diode was determined by $\log J/V$–V plot and was found to be 2.75×10^{19} eV^{-1} cm^{-3}. Capacitance–voltage measurements were performed on Al/Ta_2O_5/Al structure. The effects of biasing voltage, temperature and frequency have been investigated. The results show that the capacitance of Al/Ta_2O_5/Al MIM structure was quite sensitive to temperature and biasing voltage. The dependence of the Al/Ta_2O_5/Al structure on biasing voltage and temperature is attributed to the increase in the electron concentration as the bias voltage and temperature increase. The special conclusion in this work is to focus how the method of trap can affect the properties of the J–V characteristics. Capacitance–voltage (C–V) and current–voltage (J–V) measurements are used to characterize electrical behavior of the Al/Ta_2O_5/Al MIM structure.

References

[1] S. Ezhilvalavan, T.Y. Tseng, *J. Mater. Sci. Mater. Electron.* **10**, 9 (1999).

[2] S.V. Jagadeesh Chandra, S. Uthanna, G. Mohan Rao, *Appl. Surf. Sci.* **254**, 1953 (2008).

[3] Y.S. Shin, J.Y. Kim, C.M. Wang, J.F. Bonnet, K. Scott Weil, *Surf. Sci.* **603**, 2290 (2009).

[4] M. Stromme Mattsson, G.A. Niklasson, *J. Appl. Phys.* **85**, 8199 (1999).

[5] C.G. Granqvist, *Handbook of Inorganic Electrochromic Materials*, Elsevier, Amsterdam 1995, p. 408.

[6] J.Y. Zhang, I.W. Boyd, *Appl. Surf. Sci.* **168**, 234 (2000).

[7] J.Y. Zhang, B. Lim, V. Dusastre, I.W. Boyd, *Appl. Phys. Lett.* **73**, 2299 (1998).

[8] J.Y. Zhang, I.W. Boyd, *Appl. Phys. A* **70**, 1 (2000).

[9] W.H. Cheng, S.F. Chi, A.K. Chu, *Thin Solid Films* **347**, 233 (1999).

[10] H. Takahashi, S. Suzuki, I. Nishi, *J. Lightwave Technol.* **12**, 989 (1994).

[11] H. Terui, M. Kobayashi, *Appl. Phys. Lett.* **32**, 666 (1978).

[12] H. Shinriki, M. Nakata, *IEEE Trans. Electron Dev.* **38**, 455 (1991).

[13] F. Rubio, J.M. Albella, J.M. Martinz-Duart, *Thin Solid Films* **90**, 405 (1981).

[14] Y.K. Tu, C.C. Lin, W.S. Wang, S.L. Huang, *Proc. SPIE* **836**, 40 (1987).

[15] W.C. Herrmann, *J. Vac. Sci. Technol.* **18**, 1303 (1981).

[16] M.A. Mohammad, D.V. Morgan, *Phys. State A* **115**, 213 (1989).

[17] Yi-Hao Pai, Chih-Cheng Chou, Fuh-Sheng Shieu, *Mater. Chem. Phys.* **107**, 524 (2008).

[18] O.A. Azim, M.M. Abdel-Aziz, I.S. Yahia, *Appl. Surf. Sci.* **255**, 4829 (2009).

[19] O.S. Panwar, S.K. Gupta, M. Alim Khan, B.S. Satyanarayana, R. Bhattacharyya, *Diam. Relat. Mater.* **13**, 513 (2004).

[20] K.D. McKenzie, P.G. Le Comber, W.E. Spear, *Philos. Mag. B* **46**, 377 (1982).

[21] M.A. Lampert, P. Mark, *Current Injection in Solids*, Academic, New York 1970.

[22] A.M.A. Barry, *Physica B* **396**, 49 (2007).

[23] M.A. Lampert, P. Mark, *Current Injection in Solids*, Academic Press, New York 1970.

[24] F. Yakuphanoglu, N. Tugluoglu, S. Karadeniz, *Physica B* **392**, 188 (2007).

[25] R.D. Gould, *J. Appl. Phys.* **53**, 3353 (1982).

[26] V.S. Kushwaha, A. Kunar, *J. Mater. Sci.* **42**, 2712 (2007).

[27] V.S. Kushwaha, A. Kunar, *Mater. Lett.* **60**, 2148 (2006).

[28] www.ece.utep.edu/courses/ee3329/ee3329/Studyguide/ToC/F

[29] *PV-2000-4*, Eds. K.R. Hebert, R.S. Lillard, B.R. MacDougall, The Electrochemical Society, Pennington, NJ 2000.

[30] H. Hu, C. Zhu, Y.F. Lu, M.F. Li, B.J. Cho, W.K. Choi, *IEEE Electron Dev. Lett.* **23**, 514 (2002).

[31] M.A. Green, J. Shewchun, *J. Appl. Phys.* **46**, 51 (1975).

[32] D.E. Yıldız, S. Altındal, *Microelectron. Eng.* **85**, 289 (2008).

[33] Z.T. Song, N. Chong, H.L.W. Chan, C.L. Choy, *Appl. Phys. Lett.* **79**, 668 (2001).

[34] V. Fouad-Hanna, *Electron. Lett.* **16**, 604 (1980).

[35] C. Veyres, V. Fouad-Hanna, *Int. J. Electron.* **48**, 47 (1980).

[36] B.M. Xu, R.G. Polcawich, S. Trolier-Mckinstry, Y.H. Ye, L.E. Cross, J.J. Bernstein, R. Miller, *Appl. Phys. Lett.* **75**, 4180 (1999).

[37] M.A. Majeed Khan, M. Zulfequar, M. Husain, *Physica B* **366**, 1 (2005).